

Methodology

The methods involved in the measurement of B26 ionic species are extensively described in Sommer (1996) and only briefly summarized here. Ions were measured at Heidelberg University utilizing a Dionex 300 Ion Chromatographer with CS12 separation column in isocratic configuration run (15 minutes) measuring Ca^{2+} , Mg^{2+} , K^+ , NH_4^+ and Na^+ , while anions (F^- , Cl^- , SO_4^{2-} , Br^- , NO_3^- and MSA) were measured with a Dionex 4500i Ion Chromatograph with a AS11 separation column in a gradient configuration run (16 minutes), with reported limit of Detection (LOD) of 0.1-0.4 ppb for all elements.

All B17 discrete samples were analyzed at Alfred Wegener Institute in 2018. Given the melting speed of 2.8-3.5 cm/min and an average layer thickness (λ) of ca. 11 cm during the B17 melting campaign in Bern, the resulting sampling resolution was 2-6 samples per year. All samples were analysed by Capillary Ion Chromatography (Dionex ICS-5000+ HPIC) in a suppressed, reagent-free system and isocratic elution configuration that utilizes an IonPac AS18-Fast column (150 x 2 mm i.d.) for anions (F^- , Cl^- , SO_4^{2-} , Br^- , NO_3^- and MSA) and a IonPac CS12A column for cations (Ca^{2+} , Mg^{2+} , K^+ , NH_4^+ and Na^+) measurements. Accuracy has been calculated as relative standard deviation (in %) of ionic species measured in Milli-Q[®] water collected during the B17 melting campaign and it is defined as:

$$Accuracy = RSD_i = \frac{\sigma}{\mu} \cdot 100$$

where σ is standard deviation and μ is the mean of concentration of ionic species i in Milli-Q[®] water.

Similarly, precision has been calculated as the average of the relative standard deviation of ionic species measured in Milli-Q[®] water by Ion Chromatography and nominal values for Milli-Q[®] water reported in (Kano et al., 2004) and it is defined as:

$$Precision = \left[\frac{\sum_1^n \frac{\sigma}{x_i}}{n-1} \right] \cdot 100$$

where n is the number of measurements, σ is again standard deviation and x_i is the nominal concentration of the species i in Milli-Q[®] water as in (Kano et al., 2004).

Overall reproducibility (precision) and accuracy are 0.05% and 0.01% RSD respectively, maintaining the sensitivity of the conductivity detector in the range of 0.2-0.5 nS·ng·g⁻¹, resulting in a Limit of Detection (LOD) between 0.07 and 0.1 ng·g⁻¹ for most elements. Limit of Detection for each element has been calculated as in Hubaux & Vos (1970).

Figures

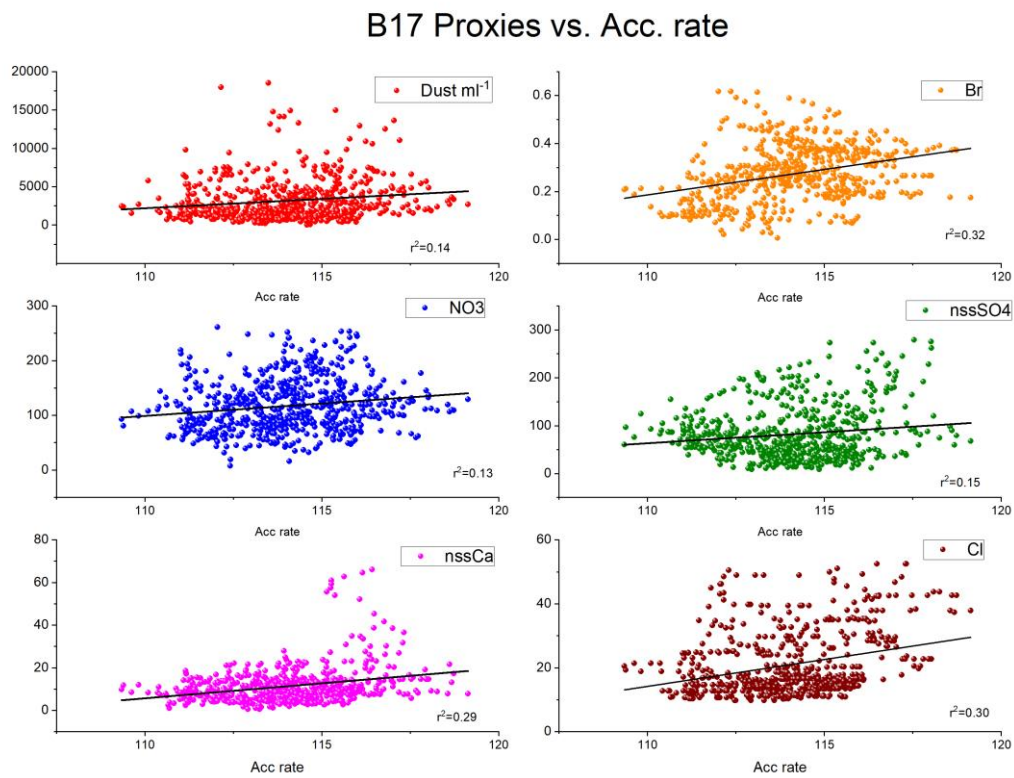


Figure s1: Relationship between Accumulation rate and concentration (in ppb) of impurities in the case of the B17 ice core record. A direct relationship, however weak ($r^2=0.13-0.32$), is observed for all the proxies shown, assessing that higher accumulation rates usually correspond to higher concentration in ice cores. We here considered $\text{nssCa}=\text{Ca}^{2+}-0.038\text{ssNa}^{2+}$ (see text) as in (Röthlisberger et al., 2002) and $\text{nssSO}_4^{2-}=\text{SO}_4^{2-}-0.052\text{Cl}$ (Mulvaney et al., 1992).

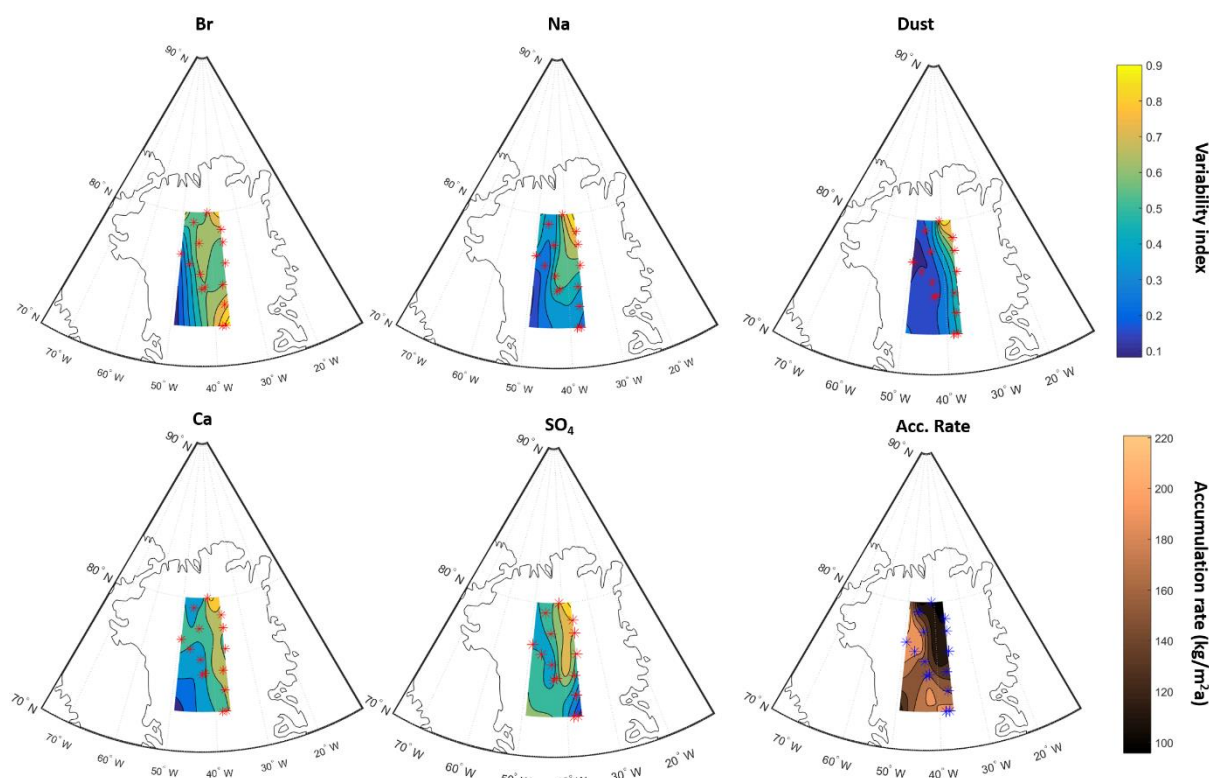


Figure s2: Variability of Impurities and accumulation rate across the NGT ice core arrays. The variability index is defined as the average amplitude of the residuals from baseline correction performed via asymmetric least square smoothing (ALSQ) as in (Peng et al., 2010). The variability of each element has been then normalized between 0 and 1 to allow the creation of contour maps. Red and Blue stars indicate the location of the ice core belonging to the NGT array utilized to create the maps. Accumulation rate for all NGT ice cores considered were obtained from (Weißbach et al., 2016). We can clearly see a trend on increasing variability going from Southwest to Northeast, opposite to average accumulation rate which is lower in the North-eastern sector (B19 & B20) than in the Southern or Western sector (B26, B27/28, B29). This confirms that low accumulation rate facilitates the occurrence of larger ranges of variability, due to a combination stronger influence of single storm events (which are naturally more variable in dust and sea salt input) and the statistical reduction of persistence and autocorrelation in a more uneven-spaced time series.

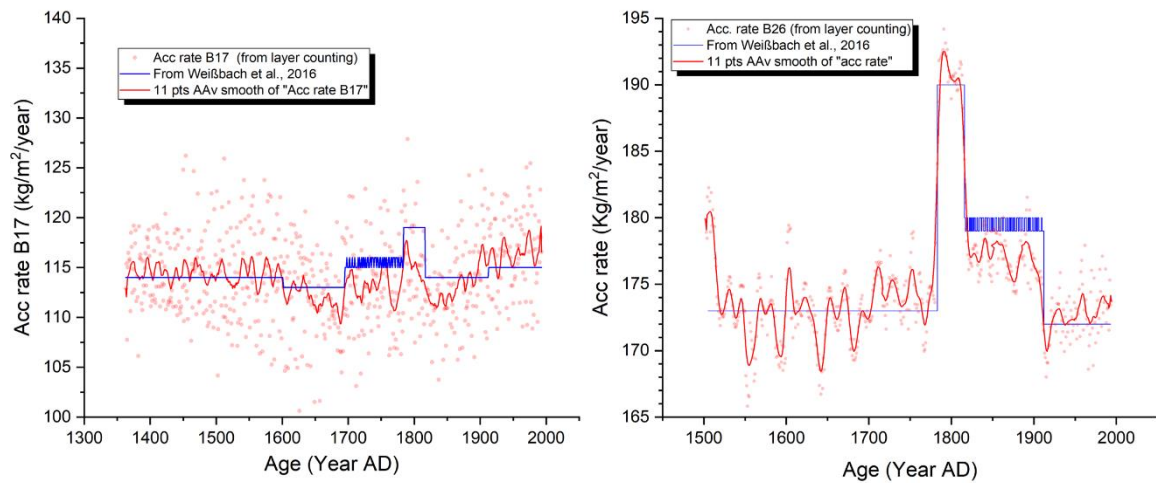


Figure s3: Accumulation rate reconstruction for the B17 (left panel) and B26 (right panel). The blue line represents the accumulation rate reconstruction performed in Weißbach et al., 2016, assuming constant accumulation rate between known time markers attributed to specific volcanic eruptions (see Weißbach et al., 2016). Based on Weißbach et al. time markers, we performed layer counting utilizing Conductivity, SO_4^{2-} , Ca^{2+} and NH_4^+ to identify layer thickness for each year. The layer thickness has been subsequently corrected according to the thinning factor: $l/L=h/H$, where l is the ice thickness of a layer, h is the height above the bed, L is the original thickness and H is the original height above the bed. Original height (H) has been estimated based on the age of the layer and the ice velocity at the ice core site utilizing data from the Greenland Ice Mapping Project from the National Snow & Ice Data Centre (Joughin et al., 2018). Original thickness (L) has been then multiplied by the Ice core density as in Wilhelms, (1996) to obtain accumulation rate in $\text{Kg}/\text{m}^2\text{a}$. We can observe a general higher accumulation rate in the B26 record compared to B17 and a larger variability as well.

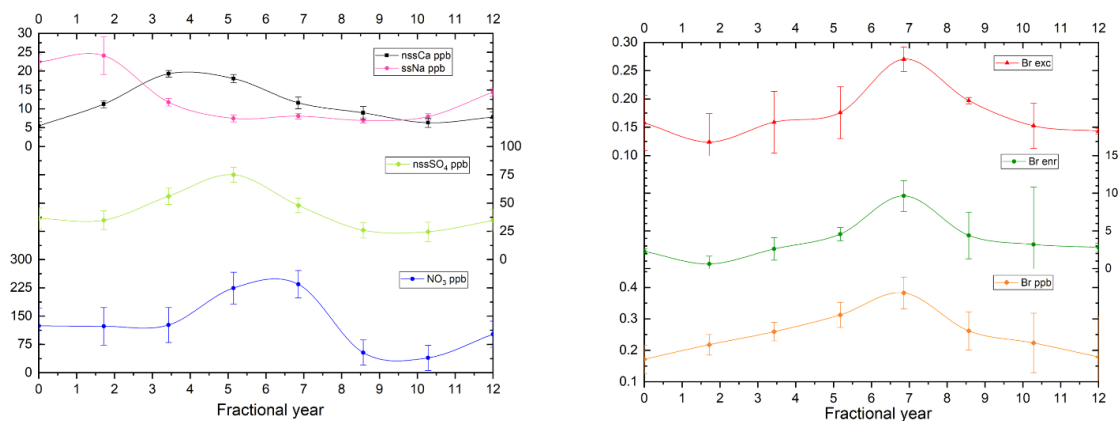


Figure s4: The seasonality of several chemical species has been investigated by averaging the original concentration profiles of every single year within the period 1790-1810 AD in the B17 ice core, where the data was sufficiently spatially resolved to achieve bi-monthly resolution. Error bars in fig. 4 represent $\pm 2\sigma$ for each value. For this time interval our maximum counting error (n° uncertain years/2) has been reduced to 0.5. This interval also follows closely a SO_4^{2-} peak corresponding to year AD 1783. Several studies have shown that sea salt transport in the Greenland region is higher during wintertime, owing to the increase storm activity over the open oceans (Fischer et al., 1998; Whitlow et al., 1992), whereas nssCa²⁺ and nssSO₄ in Greenland tend to peak in late springtime (Legrand & Mayewski, 1997) due to higher dust supply from Asian and African desert (Dibb et al., 2007). We can observe a peak of ssNa⁺ at the beginning of the profile (fractional year = 0), where values are more than twice as high as the rest of the year. The Sodium peak is followed by nssCa²⁺ (fractional year = 3-4) and a nssSO₄²⁻ maxima (fractional year =5) which again show two-fold and three-fold increase in concentrations than the rest of the year, respectively. Finally, NO₃⁻ show a three-fold concentration increase corresponding to a fractional year of 7, similarly to Bromine species, which display a three-fold increase of concentration around fractional year 7 as well. Although it is difficult to attribute specific months to a single fractional year value, the phasing of these peaks suggest that Bromine concentration increase in mid-summer, in contrast with sea salt Sodium which is well anticorrelated with Br⁻ along the year and peak in wintertime. The peak in dust supply is represented by nssCa²⁺ and marginally by nssSO₄²⁻ and is located in between ssNa⁺ and Br⁻ maxima, consistent with a springtime input. Bromine enrichment reach also a maximum in mid-summer and it is likely related with an increased lifetime of the transported aerosol which allow prolonged photolysis on the aerosol surface and therefore further enrichment of Bromine compared to Sodium. This is likely related to the fact that, in general, stronger positive Br enrichment are found in aerosol of smaller size, which indeed can travel further and present longer lifetimes (Sander et al., 2003).

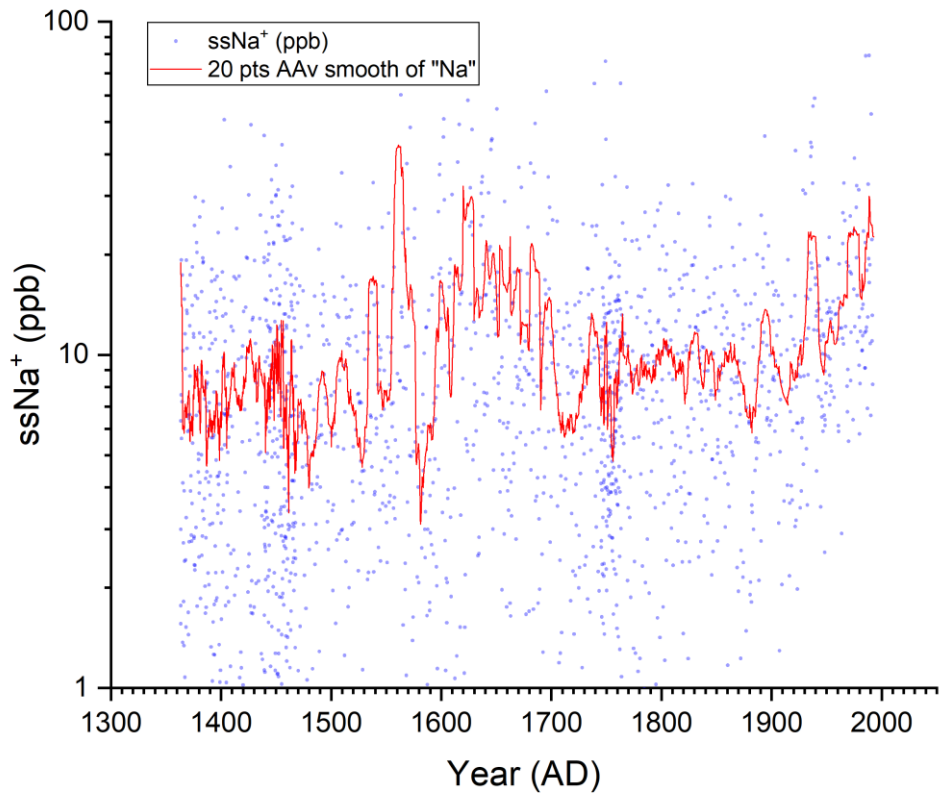


Figure s5: Concentration (in ppb) of ssNa⁺ in the B17 ice core. Blue dots are original ssNa⁺ data points, while the thick red line represent a 20-points adjacent-average smooth. We can clearly observe a general increase of ssNa⁺ AD, possibly related to the initiation of the little ice age, followed by a relative decrease in the period 1700 – 1900 AD and an increasing in the 20th century.

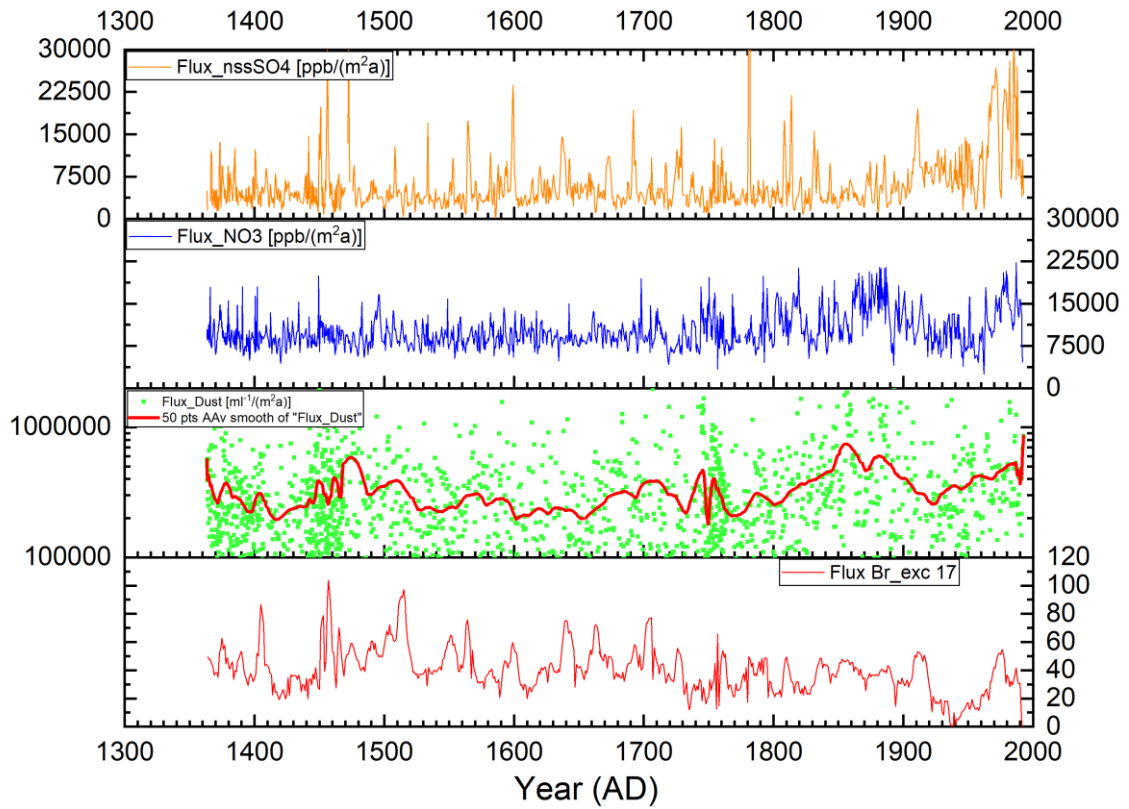


Figure s6: B17 Fluxes of: (from top) nssSO_4^{2-} , NO_3^- , Dust, Bromine-excess (Br_exc). High levels of dust and acidity (especially NO_3^-) are observed in the period 1800-1920 AD while no above-average Bromine-excess is observable in the same time interval. After 1920 AD NO_3^- is decreasing again to average values together with Bromine-excess (which reaches an overall minimum) while SO_4^{2-} show a concomitant rise around the year 1940 (AD).

References

- Dibb, J. E., Whitlow, S. I., and Arsenault, M. (2007). Seasonal variations in the soluble ion content of snow at Summit, Greenland: Constraints from three years of daily surface snow samples. *Atmospheric Environment*, 41(24), 5007–5019.
- Fischer, H., Werner, M., Wagenbach, D., Schwager, M., Thorsteinsson, T., Wilhelms, F., Kipfstuhl, J., and Sommer, S. (1998). Little Ice Age clearly recorded in northern Greenland ice cores. *Geophysical Research Letters*, 25(10), 1749–1752. <https://doi.org/10.1029/98GL01177>
- Hubaux, A., & Vos, G. (1970). Decision and detection limits for calibration curves. *Analytical Chemistry*, 42(8), 849–855. <https://doi.org/10.1021/ac60290a013>
- Joughin, I., Smith, B. E., and Howat, I. M. (2018). A complete map of Greenland ice velocity derived from satellite data collected over 20 years. *Journal of Glaciology*, 64(243), 1–11.
- Kano, I., Castillo, E., Darbouret, D., and Mabic, S. (2004). Using ultrapure water in ion chromatography to run analyses at the ng/L level. *Journal of Chromatography A*, 1039(1–2), 27–31.
- Legrand, M., & Mayewski, P. (1997). Glaciochemistry of polar ice cores: A review. *Reviews of Geophysics*, 35(3), 219. <https://doi.org/10.1029/96RG03527>
- Mulvaney, R., Pasteur, E. C., Peel, D. A., Saltzman, E. S., and Whung, P.-Y. (1992). The ratio of MSA to non-sea-salt sulphate in Antarctic Peninsula ice cores. *Tellus B*, 44(4), 295–303. <https://doi.org/10.1034/j.1600-0889.1992.t01-2-00007.x>
- Peng, J., Peng, S., Jiang, A., Wei, J., Li, C., and Tan, J. (2010). Asymmetric least squares for multiple spectra baseline correction. *Analytica Chimica Acta*, 683(1), 63–68.
- Röthlisberger, R., Mulvaney, R., Wolff, E. W., Hutterli, M. A., Bigler, M., Sommer, S., and Jouzel, J. (2002). Dust and sea salt variability in central East Antarctica (Dome C) over the last 45 kyrs and its implications for southern high-latitude climate. *Geophysical Research Letters*, 29(20), 24-1-24-4.
- Sander, R., Keene, W. C., Pszenny, A. A. P., Arimoto, R., Ayers, G. P., Baboukas, E., Caine, J. M., Crutzen, P. J., Duce, R. A., Hönninger, G., Huebert, B. J., Maenhaut, W., Mihalopoulos, N., Turekian, V. C. and Van Dingenen, R. (2003). Inorganic bromine in the marine boundary layer: a critical review. *Atmospheric Chemistry and Physics*, 3(5), 1301–1336. <https://doi.org/10.5194/acp-3-1301-2003>
- Sommer, S. (1996). *Hochauflösende Spurenstoff Untersuchungen an Eisbohrkernen aus Nord-Grönland. Diplomarbeit*. Universität Bern.
- Weißbach, S., Wegner, A., Opel, T., Oerter, H., Vinther, B. M., and Kipfstuhl, S. (2016). Spatial and temporal oxygen isotope variability in northern Greenland – implications for a new climate record over the past millennium. *Climate of the Past*, 12(2), 171–188. <https://doi.org/10.5194/cp-12-171-2016>
- Whitlow, S., Mayewski, P. A., and Dibb, J. E. (1992). A comparison of major chemical species seasonal concentration and accumulation at the South Pole and summit, Greenland. *Atmospheric Environment. Part A. General Topics*, 26(11), 2045–2054.
- Wilhelms, F. (1996). Measuring the conductivity and density of ice cores. PhD Thesis. *Reports on Polar Research*, 191. Alfred Wegener Institute.